Title: Teneurin-3 and latrophilin-2 are required for somatotopic map formation and somatosensory topognosis

Authors: Kevin T. Sangster[1,2], Xinying Zhang[1,2], Daniel del Toro[3], Christina Sarantopoulos[1,2], Ashley M. Moses[4], Shreya Mahasenan[1], Daniel T. Pederick[4], Sophie Perreault[5], Catherine Fallet-Bianco[6,7], R. Brian Roome[8], Elena Seiradake[9], Liqun Luo[4], Artur Kania[1,2,10,11 *]

Affiliations:

[1]Institut de Recherches Cliniques de Montréal (IRCM); Montréal, QC, Canada.

[2]Integrated Program in Neuroscience, McGill University; Montréal, QC, Canada.

[3]Department of Biomedical Sciences, Faculty of Medicine and Health Sciences, Institute of Neurosciences, IDIBAPS, CIBERNED; University of Barcelona, Barcelona, Spain.

[4]Department of Biology, Howard Hughes Medical Institute, Stanford University; Stanford, CA, USA.

[5]Azrieli Research Center at CHU Sainte-Justine; Montréal, QC, Canada.

[6]Department of Pathology, CHU Sainte-Justine; Montréal, QC, Canada.

[7]Department of Pathology and Cell Biology, Université de Montréal; Montréal, QC, Canada.

[8]Spinal Circuits and Plasticity Unit, National Institute of Neurological Disorders and Stroke; Bethesda, MD, USA.

[9]Department of Biochemistry, Oxford University; Oxford, UK.

[10]Division of Experimental Medicine, McGill University; Montréal, QC, Canada.

[11]Department of Anatomy and Cell Biology, McGill University; Montréal, QC, Canada.

*Corresponding author. Email: artur.kania@ircm.qc.ca

Abstract: Somatotopy is a recurring organisational feature of the somatosensory system where adjacent neurons and their connections represent adjacent regions of the body. The molecular mechanisms governing the formation of such “body maps” remain largely unknown. Here we demonstrate that the cell surface proteins teneurin-3 and latrophilin-2 are expressed in opposing gradients in multiple somatotopic maps in the mouse, including within the dorsal horn of the spinal cord. Genetic manipulation of these proteins in spinal dorsal horn or sensory neurons distorts the somatotopy of neuronal connections and impairs accurate localisation of a noxious stimulus on the surface of the body. Our work provides the foundation for a molecular model of somatotopic map formation and insights into their function in the localisation of somatosensory stimuli or topognosis.

Main Text:

Introduction

The structure of neuronal connections can reveal their functional logic. One of the organising principles of neuronal circuits are "topographic maps" which maintain the spatial relationship between a group of neurons and their post-synaptic targets. The consequence of this in the context of sensory processing is that information concerning adjacent stimuli is communicated by adjacent neurons at multiple levels of a sensory system. The classical system for studying the development of such maps has been the retinotopic map, where it has been shown that map formation is driven by specific cell surface proteins and refinement by neuronal activity (*1–8*). However, our understanding of the development of other sensory maps, particularly in the somatosensory system, remains limited.

Somatotopic maps are a unique example of topographic maps where nearby neurons represent contiguous anatomical structures. Somatotopic organisation is characteristic of most vertebrate somatosensory regions, including but not limited to the dorsal horn of the spinal cord (DH) (*9–11*), dorsal column nuclei (*12–14*), ventrobasal thalamus (*15*, *16*), and primary somatosensory cortex (*17*, *18*). The rodent DH exhibits a mediolateral (ML) organisation that corresponds to the proximodistal (PD) axis of the body where the medial dorsal horn receives sensory inputs from distal regions (e.g. the paw), while the lateral dorsal horn corresponds to more proximal regions of the body (e.g. the shoulder/hip to midline) (*9–11*). The ML map is oriented orthogonally to the dorsal horn laminae that receive modality-specific sensory afferents (*19*, *20*); the result is a columnar-like architecture where a vertical "columel" processes noxious, thermal, and light touch information originating in a particular position on the surface of the body (*21*, *22*). This somatotopic map reflects both the neuronal activity induced by sensory stimuli (*22–27*), and the organisation of incoming sensory afferents (*10*, *11*, *28*).

Despite the discovery of somatotopic maps over a century ago and much speculation as to their role in internal representation of our bodies, the mechanisms that underlie their development remain poorly understood (*17*, *29–31*). It is known that neuronal activity plays a critical role in the refinement of developing ST maps (*32–34*). On the other hand, afferent sensory axons show somatotopic organisation immediately upon entry into the DH, suggesting a contribution by hard-wiring molecular signals (*28*, *35–38*). However, the identity of such cues has remained elusive: none of the classical neuronal connectivity molecules appear to be involved despite their extensive study. Here, we identify cell surface proteins teneurin-3 (Ten3) and latrophilin-2 (Lphn2) as being essential cues for the formation of the DH somatotopic map.

Ten3 and Lphn2 expression reflects the ST organisation of the DH

Recent work has shown that heterophilic repulsion mediated by Ten3 and Lphn2, in combination with Ten3-Ten3 homophilic attraction, establish a point-to-point topography of neuronal connections in the hippocampus (*39–41*). To determine whether Lphn2 and Ten3 could direct the development of DH connectivity, we examined their expression in the mouse lumbosacral DH at embryonic day 14.5 (e14.5), when cutaneous afferents begin their entry into spinal laminae I through IV (*42*, *43*). There, we observed complementary mRNA gradients that spanned the limb somatotopic map: *Lphn2* mRNA expression was high in the medial DH (subserving the distal limb) and low in the lateral DH, while *Ten3* mRNA expression was high in the lateral DH (subserving the proximal limb) and low in the medial DH (Fig. 1A). Analysis of

protein expression using an anti-Ten3 antibody (*39*) and *Lphn2-mVenus* knock-in mice (*44*) revealed similar mediolateral gradients (Fig. 1B).

Although there is no somatotopic organisation of DRG neurons within individual ganglia, different ganglia innervate distinct patches of skin termed "dermatomes" (*9*, *45*, *46*). Correspondingly, we did not observe any spatial bias to *Ten3* or *Lphn2* expression in individual ganglia along either the dorsoventral or mediolateral axes (fig. S1A). On the other hand, we did observe an inverse relationship between *Ten3* and *Lphn2* mRNA levels in individual DRG neurons, where those that expressed a high level of *Ten3* mRNA, also expressed low levels of *Lphn2* and vice versa (fig. S1B). Additionally, DRG neurons that predominantly express either *Ten3* or *Lphn2* could be identified across all major sensory neuron subtypes (fig. S1C).

Reflecting the dermatome organisation, ganglia enriched in distal hindpaw-innervating neurons, such as L3-5, tended to have high *Lphn2* and low *Ten3* levels of expression. Conversely, ganglia enriched in more proximally-projecting neurons, such as L1-2 and L6, tended to have low Lphn2 and high Ten3 levels of expression (Fig. 1C). Thus, the level of sensory neuron expression of Lphn2 and Ten3 correlated with DH Lphn2 and Ten3 gradients and the somatotopic map of limb: distal limb sensory neurons that innervate the *Lphn2*-high medial DH express high levels of *Lphn2*, and proximal sensory neurons that innervate the *Ten3*-high lateral DH express high levels of *Ten3*. A similar correlation could be made between the protein gradients in the DRG axons located in the dorsal root entry zone (DREZ) immediately outside the DH and the gradients in the DH (Fig. 1B, quantified in fig. S1D). Next, to identify if Ten3 and Lphn2 gradients align with somatotopic maps in other somatosensory regions, we examined *Ten3* and *Lphn2* expression in the ventrobasal (VB) thalamus (postsynaptic to projection neurons in the DH) and uncovered a similar gradient that aligned with the VB somatotopic map (fig. S1E). Finally, to examine whether such Ten3/Lphn2 gradients are evolutionarily conserved we examined the expression of *TENM3* and *ADGRL2* mRNAs, encoded by the human homologues of mouse Ten3 and Lphn2, in the human fetal dorsal horn and observed similar mediolateral gradients (fig. S1F). Therefore, *Ten3* and *Lphn2* are expressed in gradients along the proximodistal axis of somatotopic maps in a conserved manner across the somatosensory system.

Ten3 and Lphn2 are required for the somatotopy of sensory afferents

Based on the observed expression patterns in the DH and DRG, as well as the previously described functions of these proteins (*40*), we hypothesized the following (Fig. 1D): (1) repulsion from Ten3 in the DH acting on Lphn2 in DRG axons directs distal limb afferents to the medial DH, (2) a combination of repulsion from Lphn2 in the medial DH acting on Ten3 in the DRG axons and attraction from Ten3 in the lateral DH acting on Ten3 in DRG axons cooperate to direct proximal limb afferents to the lateral DH. To test our hypothesis, we first challenged DRG axons with purified $Lphn2^{Lec}$ (the Teneurin-binding lectin domain) and Ten3 proteins. We found that both $Lphn2^{Lec}$ and Ten3 are repulsive to DRG axons *in vitro* (fig. S2), thereby demonstrating that Ten3 and Lphn2 are capable of guiding DRG axons. Next, we generated conditional knockouts (cKOs) of *Ten3* and *Lphn2* in the DRG and DH (fig. S3A; see methods), hereby referred to as $Ten3^{\Delta DRG}$, $Lphn2^{\Delta DRG}$, $Ten3^{\Delta DH}$, and $Lphn2^{\Delta DH}$. To assess the distribution of sensory afferents along the mediolateral extent of the DH, we co-injected cholera toxin subunit B (CTB) and wheat germ agglutinin (WGA) subcutaneously to the hindpaw or dorsal midline. These preferentially label myelinated (e.g. innocuous touch) and unmyelinated (e.g. pain and temperature) sensory afferents, respectively (*11*, *34*, *47*).

First, we examined distal limb afferent inputs to the DH, which we hypothesized to be guided by Ten3 (DH) → Lphn2 (DRG) repulsion. We therefore examined these afferents in Ten3$^{\Delta DH}$ and Lphn2$^{\Delta DRG}$ cKO mice compared to littermate controls by injecting CTB/WGA into the hindpaw and quantified the distribution of the labelled axons along the ML and superficial-deep (SD) axes of the DH (fig. S3B). In wild-type mice, the paw representation is disproportionally large and duplicated at the most medial extreme of the dorsal horn (*11*, *22*, *34*, *48*). In our controls, we saw the expected wild-type distribution of afferents however in Ten3$^{\Delta DH}$ cKO mice we observed a dramatic shift in the ML distribution of labelled afferents (Fig. 2, A to C and fig. S3C). Meanwhile, CTB and WGA-labelled axons remained in register along the ML axis (fig. S3D), and there was no shift in the distribution of CTB and WGA-labelled axons along the orthogonal SD axis (fig. S3, E to G). The Lphn2$^{\Delta DRG}$ cKO mice exhibited a milder but significant shift along the ML axis and no change in the SD axis distribution or in the ML alignment between CTB and WGA-labelled afferents (Fig. 2, D to F and fig. S3, H to L).

We next examined proximal afferent inputs to the DH, which we hypothesize are guided by a combination of Lphn2 (DH) → Ten3 (DRG) repulsion and Ten3 (DH) → Ten3 (DRG) attraction. We therefore examined these afferents in Ten3$^{\Delta DH}$, Lphn2$^{\Delta DH}$, and Ten3$^{\Delta DRG}$ cKO mice and compared them to littermate controls by injecting CTB/WGA subcutaneously at the dorsal midline. Like for the distal limb afferents, we observed a dramatic shift in the ML distribution of proximal afferents in the Ten3$^{\Delta DH}$ cKO mice (Fig. 3, A to C and fig. S4A). However, this was accompanied by a decrease in the ML alignment of the CTB with the WGA-labelled afferents (fig. S4B), and an expansion in the SD distribution of both classes of afferents (fig. S4, C to E). Lphn2$^{\Delta DH}$ cKO mice exhibited a comparatively mild but significant shift along the ML and SD axes, without a consequence on the alignment of CTB with the WGA-labelled afferents (Fig. 3, D to F and fig. S4, F to J). Unexpectedly, the Ten3$^{\Delta DRG}$ cKO mice did not exhibit any significant changes in the targeting of afferents in the DH (Fig. 3, G to I and fig. S4, K to O), indicating that Ten3 in the DRG may be dispensable for correct somatotopic and laminar targeting. Importantly, Ten3 (DH) → Lphn2 (DRG) repulsion is likely intact in Ten3$^{\Delta DRG}$ cKO mice, suggesting that this repulsion alone may be sufficient to separate the distal and proximal inputs along the ML axis. Together, our cKO experiments demonstrate that Ten3 and Lphn2 are essential for the correct somatotopic organisation of primary sensory afferents in the DH, with the severity of miswiring phenotypes depending on the ablated gene and targeted tissue.

Computational modelling of somatotopic map formation in the DH

To better understand our observed phenotypes and gain further insights into the developmental programs that produce the DH somatotopic map, we sought to construct a comprehensive computational model of DH somatotopic map formation. Over the past 40 years, several computational models of topographic map formation in the visual system have been developed and iteratively improved with experimental data. We first sought to determine if these theoretical models of topographic map formation could be applied to somatotopic maps. We therefore adapted the Koulakov model (*8*, *49*, *50*) (see methods) as it is a relatively abstract model without excessive constraints regarding the cellular mechanisms. It also effectively predicts the observed effects of genetic manipulations (*51*), and incorporates guidance cues, competition, and activity-dependent refinement into a single unified model (*8*). After adapting this model to the DH somatotopic map, we then performed Bayesian Simulation-Based Inference (SBI) using the Sequential Monte Carlo method for Approximate Bayesian Computation (ABC-

SMC) to identify parameter values for our model that fit both the observed control and cKO data in an unbiased manner (Fig. 4A; see methods).

We first confirmed that this model was able to accurately reproduce the proximal → lateral and distal → medial connectivity between DRG and DH neurons under wild-type conditions (Fig. 4B and fig. S5A). We then confirmed we were able to closely recapitulate the observed distributions of CTB/WGA along the ML axis in both controls and all cKOs examined experimentally above (Fig. 4C). Inspection of the parameter values (table S1) reveals that the best fitting model incorporates a prominent role for activity-dependent refinement of connectivity, consistent with previous experimental results (*32–34*). Furthermore, disrupting activity dependent refinement in our model produced qualitatively similar broadening of DRG axon terminal zones and disruptions to DH somatotopy as what is observed experimentally (fig. S5, B to D). Our model also indicates that there is strong competition between DRG axons for limited space in the DH along the ML axis, consistent with previous results showing an expansion of the saphenous nerve afferent termini when the afferents of the sciatic nerve are eliminated (*52*, *53*). We recreated this experiment *in silico* by ablating proximal limb DRG neurons and observed a similar expansion of the remaining axons to fill the available ML extent of the DH (fig. S5, E and F). Additional inferences of our model are that Ten3 (DH) → Lphn2 (DRG) repulsion plays a more prominent role than Lphn2 (DH) → Ten3 (DRG) repulsion or Ten3 (DH) → Ten3 (DRG) attraction, and that there is an effect on both guidance and activity-dependent refinement, particularly in the Ten3$^{\Delta DH}$ cKOs. Taken together, despite being developed for a different sensory system being patterned by unrelated molecular cues, theoretical models of topographic map formation in the visual system can be applied to developing somatotopic maps. We also show that our observed cKO data are consistent with the model that gradients of Ten3/Lphn2 cooperate to specify the DH somatotopic map.

Ten3$^{\Delta DH}$ cKOs exhibit an altered somatotopic distribution of neural activity and behavioural responses

Given the observed miswiring phenotypes, we sought to examine if this miswiring was accompanied by alterations in the function of DH circuitry. Towards this end, we selected the cKO with the most severe miswiring phenotype (Ten3$^{\Delta DH}$) and examined the consequence of injecting the hindpaw with formalin, a noxious stimulus that causes a somatotopically restricted induction of the neuronal activity marker c-Fos in DH neurons (*23*). Following injection of formalin into the distal regions of the hindpaw, both Ten3$^{\Delta DH}$ cKO mice and control littermates displayed a significant induction of c-Fos expression in the DH ipsilateral to the injection (fig. S6, A and B). While the control littermates showed increased c-Fos expression predominantly in the somatotopically appropriate medial region of the DH, in line with the innervation pattern from distal limb DRG afferents, the Ten3$^{\Delta DH}$ cKO mice exhibited a greater number of c-Fos-expressing cells in the lateral DH (Fig. 5, A to D). Matching the more widespread induction of c-Fos, cKO mice also had more c-Fos-expressing cells overall on the side ipsilateral to the injection when compared to control littermates (fig. S6, C to E).

In addition to being able to induce somatotopically restricted c-Fos activity, formalin injection elicits highly accurate licking of the injection site. Thus, using this paradigm we sought to examine the functional impact of somatotopic miswiring on the ability to locate a stimulus on the surface of the body, or topognosis. We first examined the precision of topognosis in Ten3 constitutive knockout (Ten3^{KO}) mice (*39*, *54*). Compared to control littermates, Ten3^{KO} mice

spent less time licking regions of the limb close to the injection site and more time licking regions of the limb farther from the injection (fig. S6, F to G), potentially indicating a deficit in their ability to precisely locate the stimulus. Meanwhile, the total duration of licking, an indication of stimulus intensity, was not different between KO and control mice (fig. S6H). However, Ten3^{KO} mice also showed defects in the ability to remove an adhesive tape placed on their hindlimbs, suggesting broad deficits in sensorimotor coordination (fig. S6, I and J). We next assessed topognosis in Ten3$^{\Delta DH}$ cKO mice given the magnitude of their anatomical miswiring phenotype. Similar to the Ten3^{KO} mice, Ten3$^{\Delta DH}$ cKO mice exhibited a reduction in time spent licking areas close to the injection and increase in time licking areas farther from the injection site (Fig. 5E and fig. S6L), indicating they also showed impaired topognosis. Again, this phenotype was not accompanied by any significant changes in total licking duration (fig. S6K). Finally, unlike the Ten3^{KO} mice, Ten3$^{\Delta DH}$ mice performed normally in the adhesive removal assay (fig. S6, M and N), indicating a lack of defects in sensorimotor coordination.

Discussion

Our study provides foundational insights into the molecular logic of somatotopic map formation. First, our experimental observations and modelling argue that the somatotopic map formed between peripheral sensory neurons and those in the spinal DH is driven by graded expression of Ten3 and Lphn2. This complements previous studies on their role in establishing of neuronal connections through their binary or all-or-nothing attractive and repulsive signalling. Additionally, we also provide direct functional evidence of the importance of somatotopic maps in the ability to locate a stimulus on the surface of the body.

Several parallels and distinctions between our work and that on the formation of retinotopic maps can also be made. Like in retinotopic maps, past studies and this work suggest that axon-axon interactions such as pre-ordering prior to arrival in target area and inter-axon competition, as well as activity-dependent refinement, play an important role in the establishment of the DH somatotopic map. However, the nature of the miswiring phenotypes observed by us differs significantly from those following Eph/ephrin signalling manipulations in the retinocollicular system. While Eph/ephrin signalling loss largely result in the formation of additional compact terminal zones of retinal axons in the superior colliculus (*4*, *5*, *55*), we generally observe broadening and/or shifting of sensory axon terminal zones in the ML axis of the DH, without the formation of any additional ones, suggesting the potential for fundamental cellular/molecular differences between these processes. Of particular interest would be the significance of Ten3/Lphn2 and Eph/ephrins gradient co-expression, the latter of which has been implicated in somatosensory cortex somatotopic map formation afferent thalamic axon connectivity (*56*, *57*). Finally, the presence of Ten3/Lphn2 gradients in many regions of the developing nervous system raises the possibility that they pattern all somatotopic maps within the somatosensory system, and more generally, circuits whose organising principle requires the preservation of spatial relationship between neurons and their targets (*58*).

Although we cannot rule out other DH functions of Ten3 contributing to the impaired topognosis phenotype, the unchanged duration of licking in response to formalin in Ten3$^{\Delta DH}$ cKOs suggests that stimulus intensity and location can be dissociated, echoing the idea of parallel motivational/affective and discriminatory systems underlying nociception (*59*). Importantly, our data provide some of the only functional evidence supporting the importance of somatotopic maps in somatosensory function since Penfield's original experiments involved

stimulating cortical neurons and do not allow any inferences regarding the functional requirement of somatotopic maps (*17*). Our genetics-based precise manipulation of a somatotopic map provides a new potential inroad into questions such as map plasticity, the integration of somatotopic somatosensory maps with somatotopic motor maps, or those of other sensory modalities, and their overall function in representing our bodies and whole body action planning (*31*).

References and Notes

1. R. W. Sperry, Chemoaffinity in the orderly growth of nerve fiber patterns and connections*. *Proceedings of the National Academy of Sciences* **50**, 703–710 (1963).

2. J. Walter, B. Kern-Veits, J. Huf, B. Stolze, F. Bonhoeffer, Recognition of position-specific properties of tectal cell membranes by retinal axons in vitro. *Development* **101**, 685–696 (1987).

3. H. T. Cline, M. Constantine-Paton, NMDA receptor antagonists disrupt the retinotectal topographic map. *Neuron* **3**, 413–426 (1989).

4. J. Frisén, P. A. Yates, T. McLaughlin, G. C. Friedman, D. D. M. O'Leary, M. Barbacid, Ephrin-A5 (AL-1/RAGS) Is Essential for Proper Retinal Axon Guidance and Topographic Mapping in the Mammalian Visual System. *Neuron* **20**, 235–243 (1998).

5. D. A. Feldheim, Y.-I. Kim, A. D. Bergemann, J. Frisén, M. Barbacid, J. G. Flanagan, Genetic Analysis of Ephrin-A2 and Ephrin-A5 Shows Their Requirement in Multiple Aspects of Retinocollicular Mapping. *Neuron* **25**, 563–574 (2000).

6. A. Brown, P. A. Yates, P. Burrola, D. Ortuño, A. Vaidya, T. M. Jessell, S. L. Pfaff, D. D. M. O'Leary, G. Lemke, Topographic Mapping from the Retina to the Midbrain Is Controlled by Relative but Not Absolute Levels of EphA Receptor Signaling. *Cell* **102**, 77–88 (2000).

7. T. Rashid, A. L. Upton, A. Blentic, T. Ciossek, B. Knöll, I. D. Thompson, U. Drescher, Opposing Gradients of Ephrin-As and EphA7 in the Superior Colliculus Are Essential for Topographic Mapping in the Mammalian Visual System. *Neuron* **47**, 57–69 (2005).

8. J. W. Triplett, C. Pfeiffenberger, J. Yamada, B. K. Stafford, N. T. Sweeney, A. M. Litke, A. Sher, A. A. Koulakov, D. A. Feldheim, Competition is a driving force in topographic mapping. *Proceedings of the National Academy of Sciences* **108**, 19060–19065 (2011).

9. G. Grant, J. Ygge, Somatotopic organization of the thoracic spinal nerve in the dorsal horn demonstrated with transganglionic degeneration. *Journal of Comparative Neurology* **202**, 357–364 (1981).

10. Y. Takahashi, T. Chiba, M. Kurokawa, Y. Aoki, Dermatomes and the central organization of dermatomes and body surface regions in the spinal cord dorsal horn in rats. *Journal of Comparative Neurology* **462**, 29–41 (2003).

11. K. Odagaki, H. Kameda, T. Hayashi, M. Sakurai, Mediolateral and dorsoventral projection patterns of cutaneous afferents within transverse planes of the mouse spinal dorsal horn. *Journal of Comparative Neurology* **527**, 972–984 (2019).

12. S. G. Nord, Somatotopic organization in the spinal trigeminal nucleus, the dorsal column nuclei and related structures in the rat. *Journal of Comparative Neurology* **130**, 343–356 (1967).

13. S. Maslany, D. P. Crockett, M. D. Egger, Somatotopic organization of the dorsal column nuclei in the rat: transganglionic labelling with B-HRP and WGA-HRP. *Brain Research* **564**, 56–65 (1991).

14. S. L. Florence, J. T. Wall, J. H. Kaas, Somatotopic organization of inputs from the hand to the spinal gray and cuneate nucleus of monkeys with observations on the cuneate nucleus of humans. *Journal of Comparative Neurology* **286**, 48–70 (1989).

15. J. T. Francis, S. Xu, J. K. Chapin, Proprioceptive and Cutaneous Representations in the Rat Ventral Posterolateral Thalamus. *Journal of Neurophysiology* **99**, 2291–2304 (2008).

16. R. R. Tasker, L. W. Organ, P. Hawrylyshyn, Sensory Organization of the Human Thalamus. *Applied Neurophysiology* **39**, 139–153 (1976).

17. W. Penfield, E. Boldrey, Somatic motor and sensory representation in the cerebral cortex of man as studied by electrical stimulation. *Brain* **60**, 389–443 (1937).

18. F. F. Ebner, J. H. Kaas, "Chapter 24 - Somatosensory System" in *The Rat Nervous System (Fourth Edition)*, G. Paxinos, Ed. (Academic Press, San Diego, 2015; https://www.sciencedirect.com/science/article/pii/B9780123742452000243), pp. 675–701.

19. B. Rexed, The cytoarchitectonic organization of the spinal cord in the cat. *Journal of Comparative Neurology* **96**, 415–495 (1952).

20. G. Gatto, S. Bourane, X. Ren, S. Di Costanzo, P. K. Fenton, P. Halder, R. P. Seal, M. D. Goulding, A Functional Topographic Map for Spinal Sensorimotor Reflexes. *Neuron* **109**, 91-104.e5 (2021).

21. W. D. Willis, R. E. Coggeshall, *Sensory Mechanisms of the Spinal Cord* (Springer US, Boston, MA, 1991; http://link.springer.com/10.1007/978-1-4899-0597-0).

22. A. Levinsson, H. Holmberg, J. Broman, M. Zhang, J. Schouenborg, Spinal Sensorimotor Transformation: Relation between Cutaneous Somatotopy and a Reflex Network. *J. Neurosci.* **22**, 8170–8182 (2002).

23. E. Bullitt, Somatotopy of spinal nociceptive processing. *Journal of Comparative Neurology* **312**, 279–290 (1991).

24. C. Molander, J. Hongpaisan, P. Shortland, Somatotopic redistribution of c-fos expressing neurons in the superficial dorsal horn after peripheral nerve injury. *Neuroscience* **84**, 241–253 (1998).

25. T. Sugimoto, H. Ichikawa, S. Mitani, A. Hitsu, N. Tadao, Changes in c-fos induction in dorsal horn neurons by hindpaw formalin stimulation following tibial neurotomy. *Brain Research* **642**, 348–354 (1994).

26. M. Tabata, R. Terayama, K. Maruhama, S. Iida, T. Sugimoto, Differential induction of c-Fos and phosphorylated ERK by a noxious stimulus after peripheral nerve injury. *International Journal of Neuroscience* **128**, 208–218 (2018).

27. C. Warwick, J. Salsovic, J. Hachisuka, K. M. Smith, T. D. Sheahan, H. Chen, J. Ibinson, H. R. Koerber, S. E. Ross, Cell type-specific calcium imaging of central sensitization in mouse dorsal horn. *Nat Commun* **13**, 5199 (2022).

28. K. Mirnics, H. R. Koerher, Prenatal development of rat primary afferent fibers: II. Central projections. *Journal of Comparative Neurology* **355**, 601–614 (1995).

29. A. S. F. Grünbaum, C. S. Sherrington, Observations on the physiology of the cerebral cortex of some of the higher apes. (Preliminary communication.). *Proceedings of the Royal Society of London* **69**, 206–209 (1901).

30. R. Hassler, "New Aspects of Brain Functions Revealed by Brain Diseases" in *Frontiers in Brain Research*, J. D. French, Ed. (Columbia University Press, 2019; http://www.degruyterbrill.com/document/doi/10.7312/fren91252-011/html), pp. 242–288.

31. E. M. Gordon, R. J. Chauvin, A. N. Van, A. Rajesh, A. Nielsen, D. J. Newbold, C. J. Lynch, N. A. Seider, S. R. Krimmel, K. M. Scheidter, J. Monk, R. L. Miller, A. Metoki, D. F. Montez, A. Zheng, I. Elbau, T. Madison, T. Nishino, M. J. Myers, S. Kaplan, C. Badke D'Andrea, D. V. Demeter, M. Feigelis, J. S. B. Ramirez, T. Xu, D. M. Barch, C. D. Smyser, C. E. Rogers, J. Zimmermann, K. N. Botteron, J. R. Pruett, J. T. Willie, P. Brunner, J. S. Shimony, B. P. Kay, S. Marek, S. A. Norris, C. Gratton, C. M. Sylvester, J. D. Power, C. Liston, D. J. Greene, J. L. Roland, S. E. Petersen, M. E. Raichle, T. O. Laumann, D. A. Fair, N. U. F. Dosenbach, A somato-cognitive action network alternates with effector regions in motor cortex. *Nature* **617**, 351–359 (2023).

32. B. Mendelson, Chronic embryonic MK-801 exposure disrupts the somatotopic organization of cutaneous nerve projections in the chick spinal cord. *Developmental Brain Research* **82**, 152–166 (1994).

33. S. Beggs, C. Torsney, L. J. Drew, M. Fitzgerald, The postnatal reorganization of primary afferent input and dorsal horn cell receptive fields in the rat spinal cord is an activity-dependent process. *European Journal of Neuroscience* **16**, 1249–1258 (2002).

34. M. Granmo, P. Petersson, J. Schouenborg, Action-Based Body Maps in the Spinal Cord Emerge from a Transitory Floating Organization. *J. Neurosci.* **28**, 5494–5503 (2008).

35. C. L. Smith, The development and postnatal organization of primary afferent projections to the rat thoracic spinal cord. *Journal of Comparative Neurology* **220**, 29–43 (1983).

36. M. Fitzgerald, Prenatal growth of fine-diameter primary afferents into the rat spinal cord: A transganglionic tracer study. *Journal of Comparative Neurology* **261**, 98–104 (1987).

37. I. Silos-Santiago, B. Jeng, W. D. Snider, Sensory afferents show appropriate somatotopy at the earliest stage of projection to dorsal horn: *NeuroReport* **6**, 861–865 (1995).

38. M. J. Arcaro, P. F. Schade, M. S. Livingstone, Body map proto-organization in newborn macaques. *Proceedings of the National Academy of Sciences* **116**, 24861–24871 (2019).

39. D. S. Berns, L. A. DeNardo, D. T. Pederick, L. Luo, Teneurin-3 controls topographic circuit assembly in the hippocampus. *Nature* **554**, 328–333 (2018).

40. D. T. Pederick, J. H. Lui, E. C. Gingrich, C. Xu, M. J. Wagner, Y. Liu, Z. He, S. R. Quake, L. Luo, Reciprocal repulsions instruct the precise assembly of parallel hippocampal networks. *Science* (2021).

41. E. C. Gringrich, D. T. Pederick, Y. Zhang, L. Luo, Ten3–Lphn2-mediated target selection across the extended hippocampal network demonstrates a repeated strategy for circuit assembly. bioRxiv [Preprint] (2025). https://doi.org/10.1101/2025.08.13.670207.

42. S. Ozaki, W. D. Snider, Initial trajectories of sensory axons toward laminar targets in the developing mouse spinal cord. *Journal of Comparative Neurology* **380**, 215–229 (1997).

43. H. Hasegawa, S. Abbott, B.-X. Han, Y. Qi, F. Wang, Analyzing Somatosensory Axon Projections with the Sensory Neuron-Specific Advillin Gene. *J. Neurosci.* **27**, 14404–14414 (2007).

44. G. R. Anderson, S. Maxeiner, R. Sando, T. Tsetsenis, R. C. Malenka, T. C. Südhof, Postsynaptic adhesion GPCR latrophilin-2 mediates target recognition in entorhinal-hippocampal synapse assembly. *Journal of Cell Biology* **216**, 3831–3846 (2017).

45. C. Molander, G. Grant, Cutaneous projections from the rat hindlimb foot to the substantia gelatinosa of the spinal cord studied by transganglionic transport of WGA-HRP conjugate. *Journal of Comparative Neurology* **237**, 476–484 (1985).

46. A. Prats-Galino, A. Puigdellívol-sánchez, D. Ruano-Gil, C. Molander, Representations of hindlimb digits in rat dorsal root ganglia. *Journal of Comparative Neurology* **408**, 137–145 (1999).

47. S. Maslany, D. P. Crockett, M. David Egger, Organization of cutaneous primary afferent fibers projecting to the dorsal horn in the rat: WGA-HRP versus B-HRP. *Brain Research* **569**, 123–135 (1992).

48. J. E. Swett, C. J. Woolf, The somatotopic organization of primary afferent terminals in the superficial laminae of the dorsal horn of the rat spinal cord. *Journal of Comparative Neurology* **231**, 66–77 (1985).

49. A. A. Koulakov, D. N. Tsigankov, A stochastic model for retinocollicular map development. *BMC Neurosci* **5**, 30 (2004).

50. D. N. Tsigankov, A. A. Koulakov, A unifying model for activity-dependent and activity-independent mechanisms predicts complete structure of topographic maps in ephrin-A deficient mice. *J Comput Neurosci* **21**, 101–114 (2006).

51. J. J. J. Hjorth, D. C. Sterratt, C. S. Cutts, D. J. Willshaw, S. J. Eglen, Quantitative assessment of computational models for retinotopic map formation. *Developmental Neurobiology* **75**, 641–666 (2015).

52. M. Fitzgerald, The sprouting of saphenous nerve terminals in the spinal cord following early postnatal sciatic nerve section in the rat. *Journal of Comparative Neurology* **240**, 407–413 (1985).

53. M. Fitzgerald, C. J. Woolf, P. Shortland, Collateral sprouting of the central terminals of cutaneous primary afferent neurons in the rat spinal cord: Pattern, morphology, and influence of targets. *Journal of Comparative Neurology* **300**, 370–385 (1990).

54. C. A. Leamey, S. Merlin, P. Lattouf, A. Sawatari, X. Zhou, N. Demel, K. A. Glendining, T. Oohashi, M. Sur, R. Fässler, Ten_m3 Regulates Eye-Specific Patterning in the Mammalian Visual Pathway and Is Required for Binocular Vision. *PLOS Biology* **5**, e241 (2007).

55. P. Suetterlin, U. Drescher, Target-Independent EphrinA/EphA-Mediated Axon-Axon Repulsion as a Novel Element in Retinocollicular Mapping. *Neuron* **84**, 740–752 (2014).

56. P. Vanderhaeghen, Q. Lu, N. Prakash, J. Frisén, C. A. Walsh, R. D. Frostig, J. G. Flanagan, A mapping label required for normal scale of body representation in the cortex. *Nat Neurosci* **3**, 358–365 (2000).

57. A. Dufour, J. Seibt, L. Passante, V. Depaepe, T. Ciossek, J. Frisén, K. Kullander, J. G. Flanagan, F. Polleux, P. Vanderhaeghen, Area Specificity and Topography of Thalamocortical Projections Are Controlled by ephrin/Eph Genes. *Neuron* **39**, 453–465 (2003).

58. Ur. Chon, D. T. Pederick, J. H. Song, Y. Zhang, I. Rana, L. Luo, Inverse expression of Ten3 and Lphn2 across the developing mouse brain reveals a global strategy for circuit assembly. bioRxiv [Preprint] (2025). https://doi.org/10.1101/2025.08.13.670004.

59. R. Melzack, K. Casey, Sensory, motivational, and central control determinants of pain. Kenshalo DR, editor. The skin senses: proceedings. Springfield (Illinois): Charles C. *Thomas*, 423–443 (1968).

Acknowledgments: We thank Meirong Liang for technical support; the IRCM animal facility staff; Drs. Jeffrey Mogil and Samantha Butler for comments on the manuscript; Dr. Farin Bourojeni and other members of the Kania laboratory for advice, feedback, and support. **Funding:** This work was supported by project grants from the Canadian Institutes of Health Research (CIHR; PJT-162225, MOP-77556, PJT-153053, PJT-159839, and PJT-197987) to AK and National Institutes of Health (NIH; R01-NS050580) to LL. AK holds the Doggone Foundation Chair of Excellence in Pain and receives support from the Fondation IRCM. KTS is a recipient of a CIHR doctoral scholarship (FRN:494078). XZ is a recipient of a Fonds de recherche du Québec -Santé doctoral scholarship. **Author contributions:** K.T.S. Performed all experiments except for the in-vitro and behavioural experiments, analyzed the data, and performed the computational modelling. The in-vitro experiments were performed and analyzed by D.d.T. with reagents generated by E.S. Behavioural experiments using Ten3^{KO} mice were performed by A.M.M. and D.T.P. and quantified by S.M. Behavioural experiments using Ten3$^{\Delta DH}$ mice were performed by X.Z. and quantified by C.S. R.B.R contributed to investigation and conceptualization. L.L., S.P., T.B. and C.F.B. provided reagents. A.K. supervised the study and acquired funding. A.K. and K.T.S. wrote the paper. **Competing interests:** Authors declare that they have no competing interests.

Supplementary Materials

Materials and Methods

Figs. S1 to S6

Table S1

References (60–73)

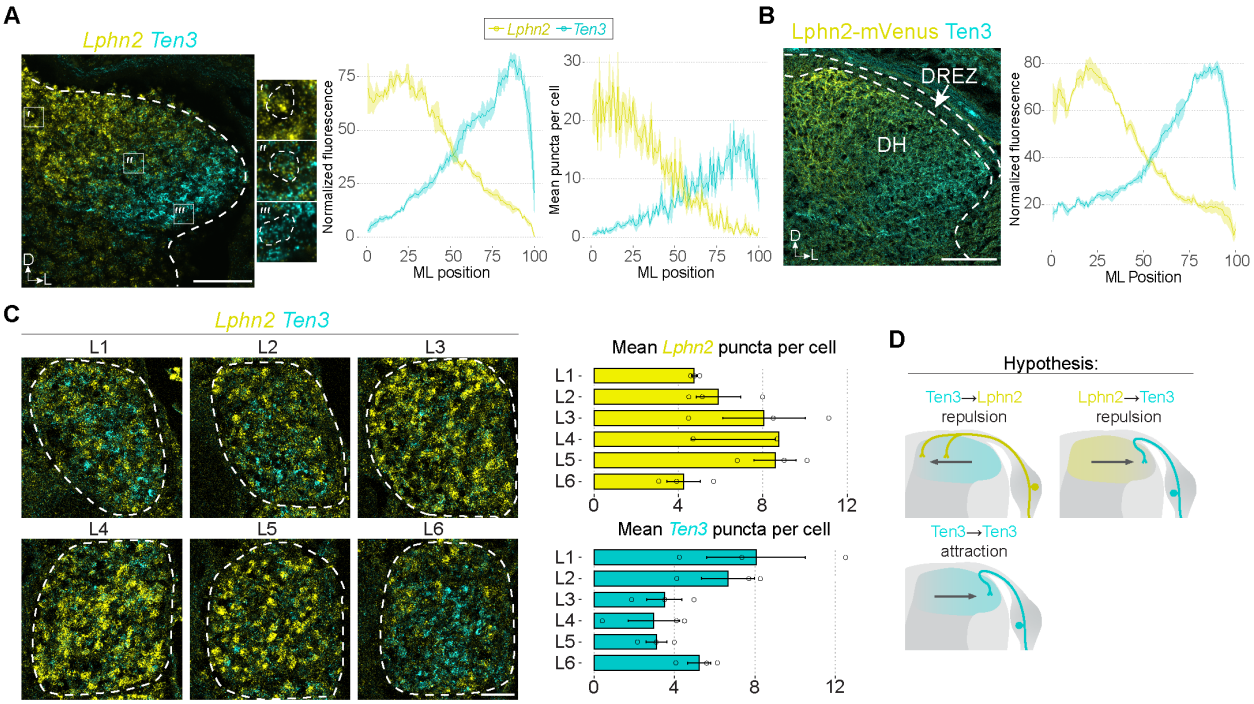

Fig. 1. Complementary expression of Ten3 and Lphn2 in the DH and DRG. (**A**) RNAscope for *Ten3* and *Lphn2* mRNA in the lumbosacral dorsal horn at e14.5 (left). Quantification of RNAscope puncta and fluorescence intensity (right, n = 4 embryos). (**B**) Immunostaining for Ten3 and Lphn2 (anti-GFP antibody) in the lumbar dorsal horn and adjacent dorsal root entry zone (DREZ) of *Lphn2-mVenus* knock-in mice at e14.5 (left). Quantification of fluorescence intensity in the DH (right, n = 3 embryos) (**C**) RNAscope for *Ten3* and *Lphn2* in lumbar dorsal root ganglia at e14.5 (left) and quantification of RNAscope puncta (right, n = 3 embryos). (**D**) Hypothesized interactions governing DH somatotopic map formation based on the expression and previously described roles of Ten3 and Lphn2. All data shown as mean ± SEM. Scale bars in A, B = 100 µm, C = 50 µm. Axis labels in this and subsequent figures: M, medial; L, ventral; D, dorsal; V, ventral.

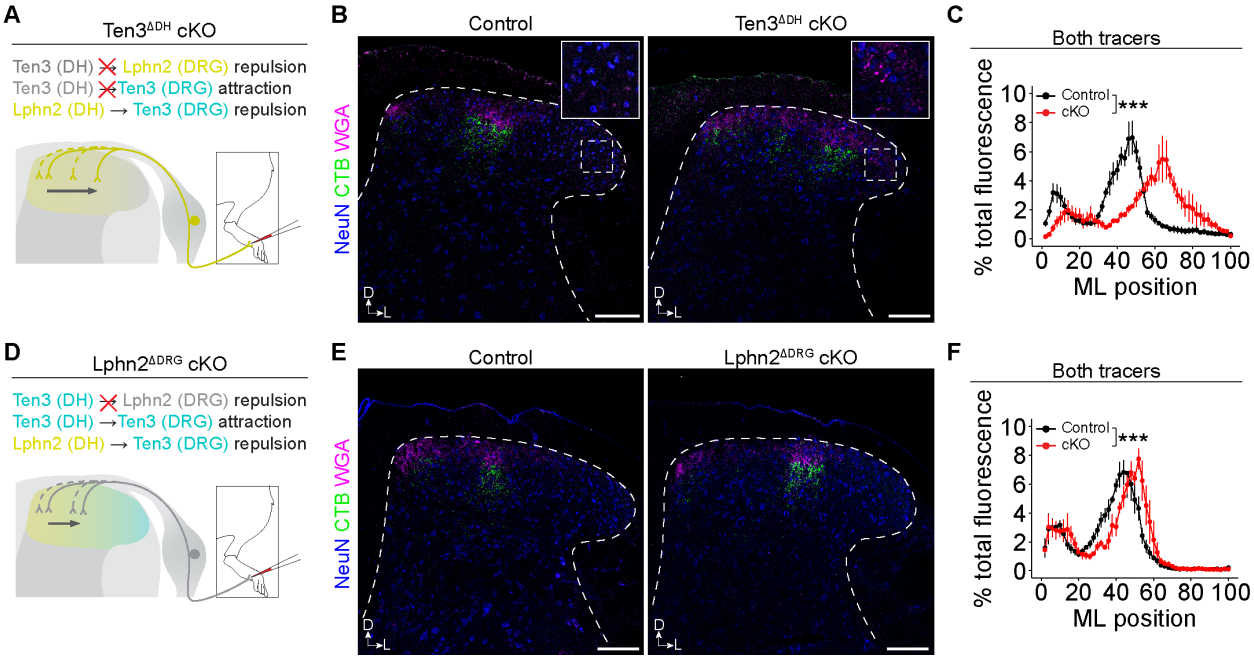

Fig. 2. Altered somatotopy of distal sensory afferents in Ten3 and Lphn2 cKOs. (**A** and **D**) Schematic of lost and preserved interactions in (A) Ten3$^{\Delta DH}$ cKOs and (D) Lphn2$^{\Delta DRG}$ cKOs (top) and the observed shift in the ST distribution of afferents in the cKOs (bottom, filled lines) compared to controls (bottom, dotted lines). (**B** and **E**) Representative images of CTB and WGA labeled afferents in (B) Ten3$^{\Delta DH}$ cKOs (insets showing WGA near lateral edge of DH in cKOs) and (E) Lphn2$^{\Delta DRG}$ cKOs compared to controls. (**C** and **F**) Quantification of the distribution of CTB and WGA signal across the ML axis of the DH in cKOs and control littermates (C) n = 4 controls, 4 cKOs, (F) n = 4 controls, 3 cKOs. All data shown as mean ± SEM. Two-way mixed ANOVA was performed and genotype x bin interaction terms are reported. ***$P \leq 0.001$; **$P \leq 0.01$; *$P \leq 0.05$. Scale bars = 100 μm.

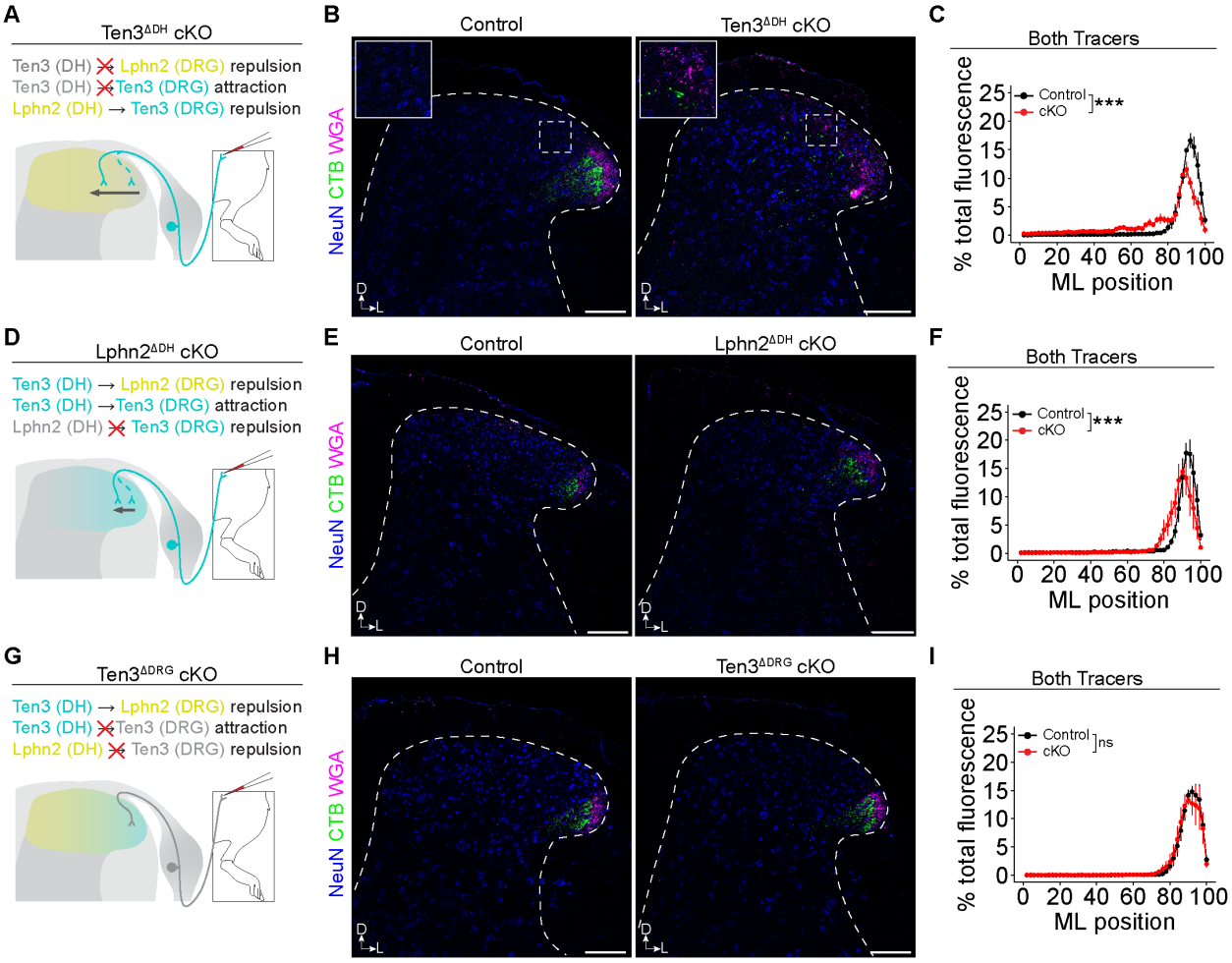

Fig. 3. Altered somatotopy of proximal sensory afferents in Ten3 and Lphn2 cKOs. (**A**, **D** and **G**) Schematic of lost and preserved interactions in (A) Ten3$^{\Delta DH}$ cKOs, (D) Lphn2$^{\Delta DH}$ cKOs, and (G) Ten3$^{\Delta DRG}$ cKOs (top) and the observed shift in the ST distribution of afferents in the cKOs (bottom, filled lines) compared to controls (bottom, dotted lines). (**B**, **E** and **H**) Representative images of CTB and WGA labeled afferents in (B) Ten3$^{\Delta DH}$ cKOs (insets show more medially located CTB/WGA in cKOs), (E) Lphn2$^{\Delta DH}$ cKOs, and (H) Ten3$^{\Delta DRG}$ cKOs compared to controls. (**C**, **F** and **I**) Quantification of the distribution of CTB and WGA signal across the ML axis of the DH in cKOs and control littermates (n = 4 controls and 4 cKOs). All data shown as mean ± SEM. Two-way mixed ANOVA was performed and genotype x bin interaction terms are reported. ***P ≤ 0.001; **P ≤ 0.01; *P ≤ 0.05. Scale bars = 100 µm.

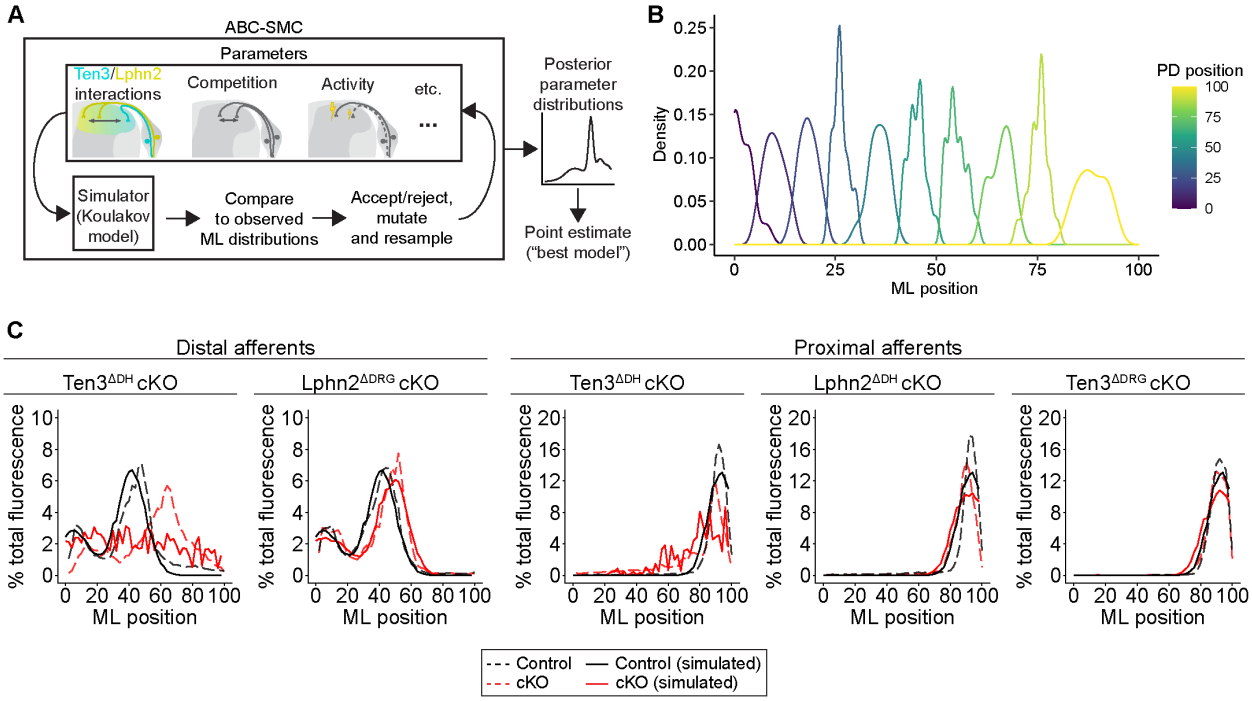

Fig. 4. Computational modelling of DH somatotopic map formation. (**A**) Simplified schematic of model parameters and ABC-SMC procedure. (**B**) Correct distal → medial and proximal → lateral mapping from one representative simulation under wild-type conditions. Simulated ML density of terminal zones in the DH from 10 DRG axons selected across the PD axis. (**C**) Observed and simulated tracer injections for controls and cKOs across all genotype/injection site combinations examined. Average distributions of each condition are shown. Simulated distribution taken from the average of 10 independent simulations.

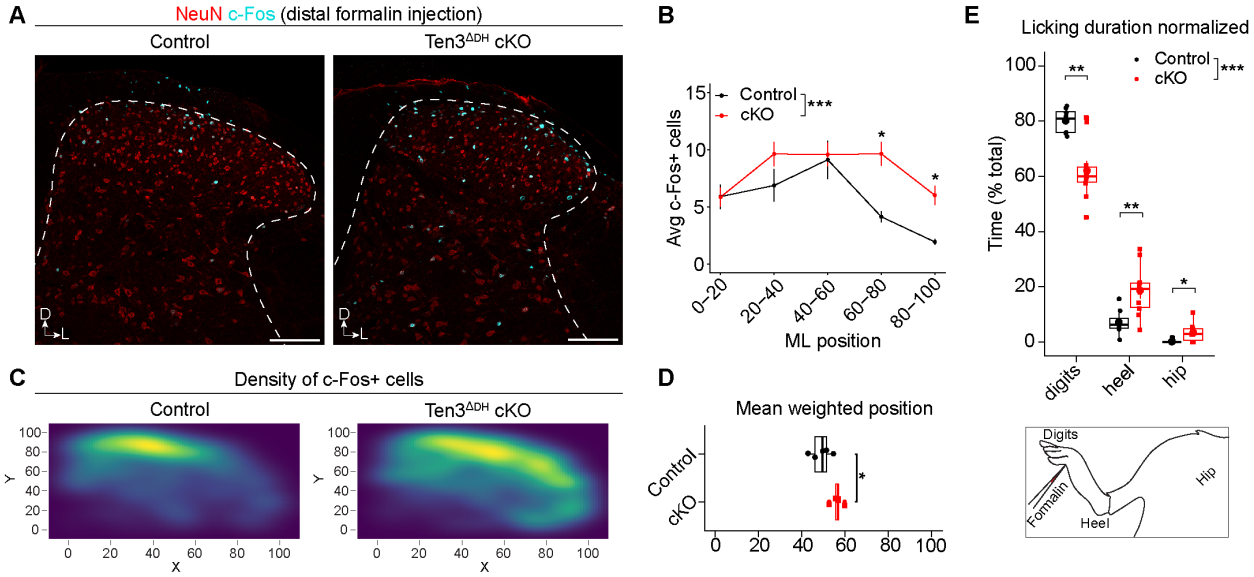

Fig. 5. Altered ST of neural activity and behavioral responses induced by a noxious stimulus in Ten3$^{\Delta DH}$ cKOs. (**A**) Representative images of immunostaining for Fos in the DH induced by formalin injection to the hindpaw of Ten3$^{\Delta DH}$ cKOs and contols. (**B-D**) Quantification of Fos positive cells in Ten3$^{\Delta DH}$ cKO mice and control littermates (n = 5 controls and 5 cKOs). (B) Distribution of Fos positive cells across the ML axis of the DH. Two-way mixed ANOVA test was performed and genotype x bin interaction term is reported along with Benjamini-Yekutieli corrected post-hoc p-values for individual bin comparisons. (C) 2D kernel density plots showing their distribution of Fos positive cells in the DH. Hotelling T^2 p-value 0.03. (D) Average ML position of Fos cells. Welch's t-test was performed. (**E**) Quantification of nocifensive licking behavior in response to formalin injection to the hindpaw near the digits, depicted as a percent of total linking time per limb region (n = 8 controls and 10 cKOs). Two-way mixed ANOVA was performed and genotype x location interaction term is reported. Post-hoc Mann-Whitney tests were performed for each limb location. All data shown as mean ± SEM. ***P ≤ 0.001; **P ≤ 0.01; *P ≤ 0.05. Scale bars = 100 µm.